OPEN ACCESS
Journal of Multidisciplinary Applied Natural Science Vol. 6 No. 1 (2026) https://doi.org/10.47352/jmans.2774-3047.310
Check for updates
Research Article

Green Synthesis of AgNPs from Argentometric Waste using *Sandoricum koetjape* Pericarp Extract: Structural Characterization and Photocatalytic Activity

Mai Anugrahwati, Endang Tri Wahyuni*, and Sri Sudiono

Received : April 25, 2025	Revised : August 1, 2025	Accepted : August 29, 2025	Online : October 4, 2025

Abstract
The growing need for sustainable nanomaterial production has driven research into more environmentally friendly synthesis methods. This study presents an innovative approach for the green synthesis of silver nanoparticles (AgNPs) by valorizing argentometric laboratory waste using *Sandoricum koetjape* (kecapi) fruit pericarp extract as a natural reducing agent. Unlike previous studies that separately investigated the chemical reduction of silver waste or plant-mediated reduction of $AgNO_3$, this work integrates both approaches. Initially, the synthesis of AgNPs from silver waste was optimized using response surface methodology with central composite design (RSM-CCD) to determine optimal reaction conditions. Then, a comparison was conducted on the resulting AgNP characteristics and performance with one synthesized from $AgNO_3$ under the same conditions. The optimized waste-derived AgNPs exhibited a crystallite size of 12 nm and an average particle size of 38.41 nm, along with a distinct surface plasmon resonance (SPR) peak at 420 nm, confirming their nanoscale formation. Comprehensive characterization by UV-Vis spectroscopy, Fourier-transform infrared spectroscopy (FTIR), XRD, TEM, and zeta potential analysis verified the nanoparticles' functionalization, stability, and crystallinity. In photocatalytic performance tests, the waste-derived AgNPs achieved 96% degradation of methylene blue, comparable to the $AgNO_3$-derived counterpart.

Keywords: green synthesis, laboratory argentometric waste, *Sandoricum koetjape*, photocatalysis

1. INTRODUCTION

The global demand for silver nanoparticles (AgNPs) continues to rise, fueled by their broad applications in healthcare and environmental technologies [1]. However, the demand is not matched by the increasing cost of silver, its primary precursor, whose price has surged due to expanding use in electronics, photovoltaics, and investment, compounded by limited production capacity [2]-[4]. This economic constraint underscores the urgency of identifying alternative, sustainable sources of silver, one promising route being the recovery of silver from waste. Equally important is adopting environmentally benign synthesis methods that avoid the use of toxic and hazardous reagents. Green synthesis, particularly plant-mediated methods, offers a sustainable pathway for AgNP production by employing phytochemicals, such as phenolics, alkaloids, polysaccharides, terpenes, and proteins, as reducing and stabilizing agents [5]-[7].

In response to these challenges, laboratory waste from argentometric experiments emerges as an overlooked but promising source of silver. This waste stream, often underutilized, typically contains high concentrations of silver in the form of AgCl and Ag_2CrO_4. Argentometric chloride determination, commonly performed using the Mohr method, is routinely conducted in undergraduate laboratories across Indonesia, with over 283 chemistry-related study programs carrying out this experiment annually [8]. It is estimated that each laboratory session generally involves 20–40 students, each using 25–50 mL of 0.1 M $AgNO_3$ per titration, corresponding to an estimated nationwide usage of 34–68 g of silver per year. Given this scale, a substantial amount of silver-containing solid waste accumulates over time, offering a sustainable source of silver for recovery and reuse. Valorizing this waste addresses two critical issues simultaneously: reducing the economic burden of AgNP production by providing a cost-effective precursor and mitigating environmental contamination by diverting heavy metal waste from disposal.

This approach can be further strengthened by integrating silver recovery with green synthesis, as

Table 1. The experimental range of independent variables (factors) used in the central composite design.

Factor	Name	Units	Min	Max	Low	High	Middle
			(-α)	(+α)	(-1)	(+1)	(0)
A	Temperature	°C	27	60	20	60	36
B	pH		8.0	12.0	8.0	12.0	10.0
C	$V_{Extract}$	mL	3.0	5.0	3.0	5.0	3.75
D	V_{Ag}	mL	1.0	2.5	1.0	2.5	1.85
E	Time	Min	11	60	11	60	20

demonstrated in several prior studies using other types of silver-containing waste. Recovered silver can be upcycled into high-value nanoparticles via plant-based green synthesis. For instance, silver leached from printed circuit boards was converted to $AgNO_3$ and immediately reduced using *Eichhornia crassipes* leaf extract, then immobilized in a chitosan matrix on cotton fabric to produce an antimicrobial textile coating [9]. Similarly, silver recovered from waste X-ray films was transformed into $AgNO_3$ and reduced with deoiled Sal seed cake extract, yielding AgNPs that efficiently catalyzed the $NaBH_4$-driven degradation of several azo dyes [10].

Among various plant-based reductants explored for green synthesis, *Sandoricum koetjape* (commonly known as kecapi or santol), a widely available medicinal plant in Southeast Asia, has shown potential due to its rich phytochemical profile. Phytochemical studies have reported the presence of tannins, alkaloids, betacyanins, and coumarins in the methanolic extract of its fruit peel [11], with tannins, betacyanins, and coumarins classified as polyphenolic compounds. These compounds are known for their antioxidant activity [11]-[14], enabling them to function as natural reducing and stabilizing agents for AgNPs [15].

Despite growing interest in both waste-derived and green-synthesized AgNPs, several key challenges remain; research efforts have treated mainly waste valorization and green synthesis as separate domains, with most studies focusing either on chemical reduction of silver waste [8][16] or plant-mediated synthesis using pure $AgNO_3$ [17]-[19]. This highlights a significant technological gap, as integrated approaches combining both strategies remain underexplored. To the best of our knowledge, only a few studies have integrated the valorization of silver waste with plant-mediated AgNP synthesis. The two notable examples discussed earlier [9][10], highlight the limited development of this approach. Moreover, due to the limited optimization and comparative studies between waste-derived and conventional AgNPs, further investigation is essential to gain a more comprehensive understanding of their respective efficiencies and catalytic performance.

Motivated by these gaps and the promising potential of *S. koetjape*, this study explores the green synthesis of AgNPs using kecapi fruit pericarp extract and silver recovered from laboratory argentometric waste. The synthesis process is systematically optimized using response surface methodology with central composite design (RSM-CCD). Using the optimized conditions, AgNPs were then synthesized under identical procedures from both waste-derived and conventional $AgNO_3$ precursors. The resulting AgNPs were characterized and compared based on their photocatalytic activity in the degradation of methylene blue. Specifically, this study aims to: (1) develop an integrated, eco-friendly synthesis route combining silver waste valorization and green chemistry; (2) implement RSM-CCD to ensure robust process optimization; and (3) provide direct comparative analyses of physicochemical characteristics and functional performance.

2. MATERIALS AND METHODS

2.1. Materials

This study utilized analytical-grade chemicals, including $AgNO_3$, NaOH, NH_3, and HNO_3 (Merck, Germany). Deionized water was used for reagent preparation, with purification performed using equipment from the Integrated Laboratory at the

Islamic University of Indonesia. Kecapi (*S. koetjape*) fruit pericarp was obtained from a vendor in West Java, Indonesia. Additionally, argentometric laboratory waste was repurposed from student laboratory activities in the Chemistry Department, Universitas Islam Indonesia, as a precursor for silver recovery and nanoparticle synthesis.

2.2. Methods

2.2.1. Preparation of Kecapi Pericarp Extract

A 5 g of dry kecapi fruit pericarp powder was added to 100 mL of deionized water. The mixture was heated at 80 °C for 15 min, then cooled and filtered using Whatman filter paper No. 1. The resulting filtrate, representing the kecapi pericarp extract, was stored in a dark bottle at 4 °C for subsequent use.

2.2.2. Preparation of Argentometric Waste

Argentometric analysis in chemistry practical

Table 2. The experimental design and the response values.

Run	Factors					Response UV (Absorbance)
	A: Temperature (°C)	B: pH	C: V_{Ag} (mL)	D: $V_{extract}$ (mL)	E: Time (min)	
1	30	9	1.00	4.00	15	0.232
2	60	11	1.00	5.00	45	0.357
3	45	10	1.50	3.00	60	0.545
4	45	10	1.50	3.00	30	0.391
5	60	11	2.00	4.00	45	0.368
6	45	10	1.50	3.00	30	0.437
7	33	10	2.00	3.75	19	0.199
8	30	9	1.50	4.25	13	0.147
9	33	10	2.00	4.75	15	0.192
10	33	10	2.00	3.75	15	0.227
11	33	10	2.00	3.75	11	0.213
12	30	11	1.50	3.25	13	0.148
13	33	10	2.00	3.75	15	0.219
14	30	11	2.50	3.25	17	0.238
15	33	10	2.00	3.75	15	0.182
16	36	9	1.50	3.25	13	0.169
17	36	9	1.50	4.25	17	0.225
18	30	11	1.50	4.25	17	0.180
19	36	9	2.50	4.25	13	0.135
20	36	9	2.50	3.25	17	0.272
21	33	12	2.00	3.75	15	0.195
22	27	10	2.00	3.75	15	0.107
23	33	10	2.00	3.75	15	0.208
24	33	8	2.00	3.75	15	0.193
25	30	9	2.50	3.25	13	0.200
26	33	10	2.00	3.75	15	0.230
27	33	10	2.00	3.75	15	0.180

Table 3. Analysis of variance for the quadratic model and fit statistics.

Source	Sum of Squares	df	Mean Square	F-value	p-value	
Model	0.2020	7	0.0289	40.6500	< 0.0001	significant
A-Temperature	0.0001	1	0.0001	0.1664	0.6881	
C-Vag	0.0022	1	0.0022	3.1400	0.0933	
D-Vex	0.0071	1	0.0071	10.0500	0.0053	
E-Time	0.0224	1	0.0224	31.6100	< 0.0001	
AD	0.0042	1	0.0042	5.8700	0.0261	
AE	0.0060	1	0.0060	8.4700	0.0093	
CD	0.0079	1	0.0079	11.0600	0.0038	
Residual	0.0128	18	0.0007			
Lack of Fit	0.0093	13	0.0007	1.0300	0.5278	not significant
Pure Error	0.0035	5	0.0007	Pure Error	0.0085	
Cor Total	0.2594	26	**Adjusted R^2**	0.9174		
R^2	0.9405		**Predicted R^2**	0.8101		

courses generates laboratory waste containing yellow liquid and solid precipitates of silver chloride (white) and silver chromate (brick red). Argentometric titration was performed according to the Mohr method under canonical conditions as described in Vogel's Quantitative Inorganic Analysis (5th ed.): 25.00 mL of 0.100 M NaCl was titrated with ~0.100 M $AgNO_3$ using 1.00 mL of 0.50 M K_2CrO_4 as indicator at 25 ± 1 °C. Based on the known solubility product of Ag_2CrO_4, the endpoint was defined at $[Ag^+] \approx 1.5 \times 10^{-5}$ M. The precipitate composition was estimated to be 99.97% AgCl and 0.03% Ag_2CrO_4, with a silver recovery efficiency of 99.97%. The precipitate serves as a precursor for synthesizing nanoparticles, which were treated with 0.1 M HCl to dissolve silver chromate, leaving silver chloride. The dried silver chloride was then dissolved in 0.01 M ammonia to form a 1 mM diamminargentate ($[Ag(NH_3)_2]^+$) complex solution predominantly [8].

2.2.3. Optimization of Green Synthesis using RSM-CCD

RSM is widely applied in chemical research due to its ability to improve process efficiency, optimize formulations, and minimize the number of experimental trials required [20]. This study employed RSM based on CCD to optimize the synthesis of waste-derived AgNPs. Five independent variables: temperature, pH, extract volume, silver nitrate solution volume, and heating time, were selected based on their distinct roles in reduction, nucleation, and growth processes, and evaluated at five levels (Table 1) with 27 experimental runs, including center and axial points. The selection of five variables in RSM has been adopted in several prior optimization studies involving green synthesis of silver nanoparticles [21][22]. The experimental data were then analyzed using Stat-Ease Design-Expert software (trial version), and ANOVA was employed to assess the significance of model terms.

For comparison, $AgNO_3$-based nanoparticles were also synthesized using the same temperature, pH, extract volume, Ag-containing solution volume (1 mM Ag^+-containing solution from $AgNO_3$), and heating time.

2.2.4. Phytochemical Analysis using Folin–Ciocalteu Method (for the Total Phenolic Content analysis), FTIR, and Nanoparticle Characterization using Spectrophotometer UV-Vis, XRD, TEM, and Zeta Potential

Total Phenolic Content (TPC) analysis was determined using the Folin–Ciocalteu method with a standard addition protocol to minimize matrix interference from other plant components. A 0.10 mL aliquot of the 20-fold diluted extract (taken from Section 2.2.1) was mixed with 0.05 mL of Folin–Ciocalteu reagent (1:10 dilution), 1.5 mL of

7.5% Na_2CO_3, and varying volumes (0, 15, 30, and 50 µL) of a 2000 ppm gallic acid (GA) standard solution. The volume was adjusted to 3.00 mL with distilled water. After 30 min of incubation, the absorbance was measured at 725 nm, corresponding to the λ_{max} of the blue molybdenum–tungsten complex [23].

The previously obtained extract was concentrated using a rotary evaporator (Eyela N-1300) at 40 °C under reduced pressure until a paste was formed, and then stored in a desiccator for further analysis. For the synthesized AgNPs, the particles were first purified through repeated centrifugation and washing, and then oven-dried before analysis. The extract paste and the dried AgNPs were analyzed for their functional groups using Fourier-transform infrared (FTIR) spectroscopy (PerkinElmer Spectrum Two), employing the KBr pellet method in the range of 400–4000 cm^{-1}. The AgNPs were also characterized using multiple techniques: UV-Vis spectrophotometry (Hitachi UH-5300) was used to analyze absorption spectra (200–700 nm), XRD (Rigaku Miniflex 600) with Cu $K\alpha_1$ radiation (λ = 1.54056 Å) was used to determine crystallinity, TEM (Jeol JEM-1400, 120 kV) was used to visualize size, morphology, and shape, and the zeta potential was measured using dynamic light scattering (Horiba SZ-100Z).

2.2.5. Photocatalytic Test

The catalytic properties of silver recovered from laboratory waste were systematically compared with those of silver synthesized from an $AgNO_3$ precursor. The photocatalytic activity was evaluated using methylene blue degradation (50 ppm, 100 mL) under three conditions: 0.25 mM H_2O_2 alone and with the addition of 25 µg/mL silver catalyst from each source. The reactions proceeded under UV irradiation (Philips TUV T8 15W low-pressure mercury lamp, emitting UV-C at 254 nm, UV-C output is 5.1 W (as specified by the manufacturer), and the distance from the lamp to the solution surface was approximately 10 cm), with degradation kinetics monitored spectrophotometrically (λ = 664 nm) at 30-min intervals over 3 h. A statistical test was performed to compare photocatalysis and analyze whether the difference was significant.

3. RESULTS AND DISCUSSIONS

3.1. Optimization

RSM with CCD was employed to systematically investigate the effects of key synthesis parameters (including five factors: temperature, pH, V_{ag} (volume of silver-containing solution), V_{ex} (volume of plant extract), and heating time) on the absorbance of the waste-derived AgNPs. In this regard, the AgNP production was measured via absorbance readings as the oscillation of electrons in metallic AgNP leads to plasmon absorption property in the visible range. A linear relationship is observed between the concentration of the

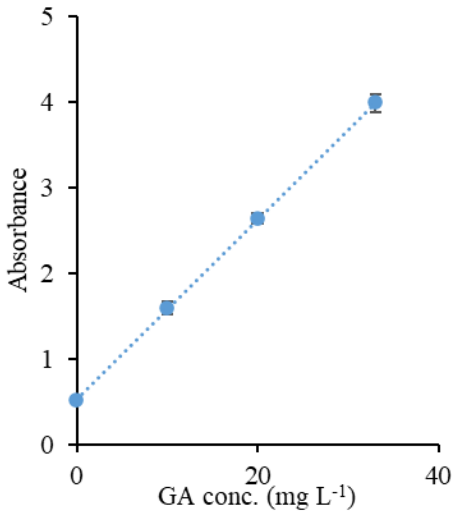

Figure 1. Calibration curve of gallic acid in the standard addition method (Folin–Ciocalteu assay), error bars represent the standard deviation of triplicate measurements.

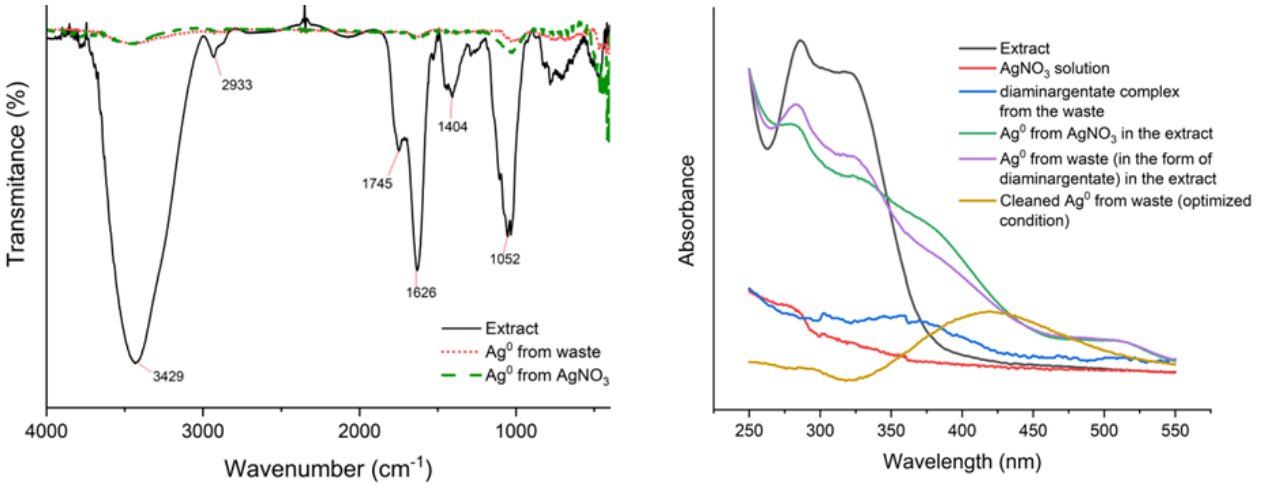

Figure 2. The analysis results include (a) FTIR spectra comparing the extract before AgNP synthesis and the green synthesized AgNPs (Ag^0) from waste and $AgNO_3$, (b) spectrophotometer UV-Vis absorbance comparison of the pericarp extract (black), $AgNO_3$ solution (red), AgCl in the ammonia solution (in the form of diaminargentate complex) (blue), the Ag^0 produced from $AgNO_3$ in the extract (green), the Ag^0 produced from the waste in the extract (purple), and cleaned waste-derived Ag^0 synthesized with the optimum condition of 45 °C, pH 10, 2.0 mL of V_{ag}, 3.0 mL of V_{ex}, and a reaction time of 60 min (yellow).

generated AgNPs and the intensity of surface plasmon resonance (SPR), indicating that this absorbance can be used to estimate AgNP concentration [24][25].

Table 2 presents the dataset generated by varying experimental parameters based on the CCD matrix, capturing both main effects and variable interactions. From the evaluation using sequential model sum of squares, lack-of-fit tests, and statistical metrics (R^2, adjusted R^2, predicted R^2, and corrected Akaike Information Criterion (AICc)), the reduced two-factor interaction (2FI) model was identified as the most suitable for fitting the response variable (absorbance). This model offers an optimal balance between goodness-of-fit and simplicity, with the highest R^2 and lowest AICc among all tested models, indicating its robustness and predictive reliability under the studied conditions.

The Anova for the reduced 2FI model (Table 3) confirms the high coefficient of determination (R^2 = 0.9405), coupled with the agreement between adjusted R^2 (0.9174) and predicted R^2 (0.8101) (the difference is less than 0.2), indicating the model's reliability. The non-significant lack of fit (p = 0.5278) and significant F-value (40.65, p = <0.0001) demonstrated that the model adequately represented the experimental data for the waste-derived AgNPs synthesis optimization. The final reduced 2FI model equation is as follows:

$$\text{Absorbance} = -1.7188 + 0.0324 \times \text{Temp (°C)} + 0.4353 \times V_{ag}\text{ (mL)} + 0.3524 \times V_{ex}\text{ (mL)} + 0.0198 \times \text{Time (min)} - 0.0048 \times \text{Temp (°C)} \times V_{ex}\text{ (mL)} - 0.00035 \times \text{Temp (°C)} \times \text{Time (min)} - 0.1161 \times V_{ag}\text{ (mL)} \times V_{ex}\text{ (mL)}$$

This model equation for the green synthesis of waste-derived AgNPs highlights key relationships between synthesis parameters and nanoparticle formation, positive coefficients for temperature, V_{ag}, V_{ex}, and reaction time suggest that increasing these variables generally promotes AgNP formation, likely due to enhanced reduction kinetics and increased collision frequency between reactants. In contrast, negative interaction for temperature × silver precursor volume (Temp.V_{ex}), temperature × time (Temp.Time), and silver precursor × reducing agent volume (V_{ag}.V_{ex}) indicate critical mechanistic constraints. These suggest that while higher temperatures accelerate reduction, excessive heat in combination with prolonged reaction time or elevated precursor concentrations may cause nanoparticle aggregation. In addition, the negative interaction between the V_{ag}.V_{ex} also implies the necessity of an optimal ratio, possibly due to the dual role of plant-derived biomolecules (as reducing and capping agents) and

a dilution effect (as total reaction volume increases, the effective concentrations of silver ions and reducing agents decrease, reducing collision frequency and slowing nanoparticle formation).

Drawing from these results, the optimized conditions for the green synthesis of waste-derived AgNp were the volume ratio of Vag/Vex of 2:3 at a temperature of 30–45 °C, pH 10, and a reaction time of 60 min, which yielded maximum absorbance (around 0.545) and desirability (=1). This study used this optimum reaction condition for waste-derived and $AgNO_3$-based nanoparticles to compare their characteristics and performance. The temperature synthesis aligns with previous findings that plant extract-based AgNP synthesis typically operates within 20–100 °C and optimally between 30–90 °C, thereby accelerating the process and producing smaller nanoparticles [26]. The pH in this synthesis must be maintained in an alkaline range to enhance the ammonia (NH_3) concentration, which will stabilize $[Ag(NH_3)_2]^+$ complexes and prevent AgCl precipitation. This will ensure a consistent supply of silver ions for reduction and optimized nanoparticle formation.

3.2. Phytochemical Analysis and Nanoparticle Characterization

Figure 1 shows the calibration curve from the standard addition assay. A linear fit (A = 0.1052 C + 0.5305, R^2 = 0.999) was obtained. The x-intercept of -5.0428 mg L^{-1} corresponds to the concentration of phenolics originally present in the diluted extract. After accounting for a 20-fold dilution of the extract and a 30-fold dilution in the assay tube, the total phenolic content in the original extract was calculated as: 5.0428 mg L^{-1} × 600 = 3025.68 mg GAE L^{-1}. Given that 5 g of dried powder was extracted in 100 mL, this corresponds to ≈ 60.51 + 2.20 mg GAE per gram of dry weight.

FTIR spectroscopy identified the functional groups involved in the reduction and capping of Ag^0 nanoparticles, as shown in Figure 2(a); major peaks were observed at 3429 (O–H), 2933 (C–H), 1746 (C=O), 1628 (C=C), 1404 (CH_2/CH_3), and 1052 (C–O/C–N) cm^{-1}, indicating the presence of a complex organic matrix. These functional groups are consistent with specific bioactive compounds found in *S. koetjape* pericarp extract, including tannins, which possess abundant phenolic –OH groups and aromatic rings; coumarins, which contain C=O and C=C groups; and anthocyanins, which exhibit characteristic C–O and C–H bands [11]. The presence of characteristic FTIR bands for O–H, aromatic C=C, and C–O [27], supports the high total phenolic content (60.51 mg GAE/g dry weight) previously quantified by the Folin–Ciocalteu assay. These findings suggest the possible involvement of phenolic compounds in the

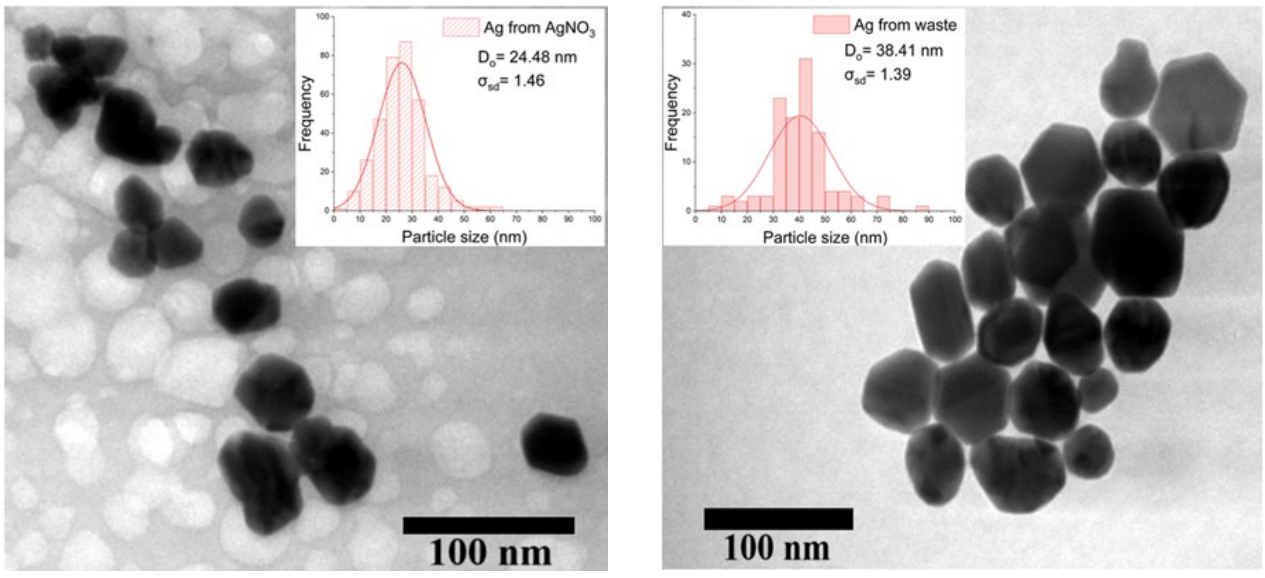

(**a**) (**b**)

Figure 3. The analysis results of (a) TEM images illustrate AgNPs from $AgNO_3$ and (b) TEM images of AgNPs from waste, both synthesized using the pericarp extract.

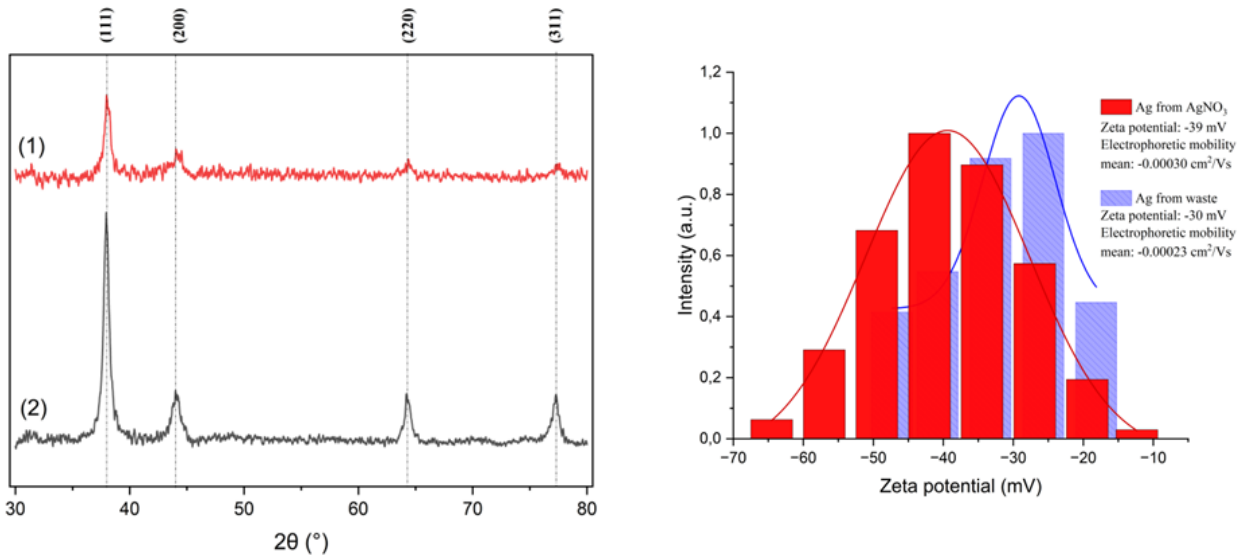

Figure 4. The analysis results of (a) XRD diffractograms of metallic Ag from $AgNO_3$ (1) and waste (2), and (b) zeta potential measurements for both AgNPs.

reduction and stabilization of AgNPs.

During the synthesis process, compounds containing O–H and C=O groups may undergo oxidation to quinones, donating electrons to reduce Ag+ in diaminargentate ion into metallic Ag^0 nanoparticles:

1. Complex formation: $Ag(NH_3)_2^+ + OH^- \rightarrow Ag(NH_3)_2OH$
2. Deprotonation: $Ar–OH \rightarrow Ar–O^- + H^+$
3. Quinone oxidation: $Ar–O^- \rightarrow Ar=O + e^-$
4. Reduction: $Ag(NH_3)_2^+ + e^- \rightarrow Ag^0 + 2NH_3$
5. Surface stabilization: $Ag^0 + Ar–OH \rightarrow Ag^0–Ar–OH$

Alternatively, phenolic compounds without the capability to oxidize to quinones reduce Ag^+ via autooxidation ($ArOH + Ag(NH_3)_2^+ \rightarrow ArO\bullet + Ag^0 + 2NH_3 + H^+$), with the reaction being accelerated in alkaline media and at elevated temperatures [26][28]. These redox processes not only enable nanoparticle formation but also contribute to their stability through capping by organic molecules, depicted in FTIR of Ag^0 (from $AgNO_3$ and waste) revealed residual O–H and C=O bands; also, C=C and C–O/C–N imply stabilization via π-electron interactions and coordination bonds, potentially involving pericarp-derived polysaccharides or glycosides [29]-[31].

Figure 2(b) presents five solutions' UV-Vis absorbance spectra (200–550 nm) in which the $AgNO_3$ curve (blue) shows no absorbance, indicating weak light absorption, and diaminargentate (black) exhibits low absorbance after 300 nm, reflecting its optical properties. The pericarp extract (red) shows a peak at 250–350 nm, attributed to π-π* and n-π* transitions in phenolic compounds [32][33]. Both Ag from $AgNO_3$ (green) and waste (purple) exhibit increased absorbance around 400–450 nm, consistent with 20–50 nm of AgNPs [34][35]. After cleanup (yellow), optimized AgNPs displayed an SPR band at 420 nm, confirming well-defined nanoscale silver formation under optimal RSM-CCD condition [36][37].

Figures 3(a) and 3(b) show TEM images of AgNPs from different synthesis methods. Ag from $AgNO_3$ formed quasi-spherical nanoparticles (D_0 = 24.48 nm, σg = 1.46), while Ag from waste exhibited polygonal nanoplatelets, faceted, laterally extended structures with nanometric thickness (<10 nm) (D_0 = 38.41 nm, σg = 1.39). To obtain the particle size distribution shown in the insets, the diameter of nanoparticles was measured from TEM micrographs using ImageJ software (by converting the TEM scale bar into pixel values and then applying the particle analysis tool).

XRD analysis (Figure 4(a)) confirms the presence of four diffraction peaks at ~38°, 44°, 64°, and 77°, corresponding to the (111), (200), (220), and (311) planes of Ag, respectively, in accordance with the JCPDS No. 04-0783 for face-centered cubic (FCC) silver [38]. The XRD patterns were

deconvoluted using a Gaussian fitting function in OriginPro 2025 (SR1; OriginLab Corporation) to obtain the full width at half maximum (FWHM) values of the diffraction peaks. For waste-based Ag, the FWHM values for the (111), (200), (220), and (311) planes were 0.6974°, 0.9997°, 0.6657°, and 0.7479°, respectively, while for $AgNO_3$-based Ag were 0.7162°, 1.3485°, 0.8097°, and 0.7806°, respectively. These values were then used to estimate crystallite size (D) using the Debye–Scherrer Equation 1 [18];

$$D = K\lambda/(\beta \cos \theta) \quad (1)$$

where λ = 0.15406 nm (Cu Kα), K= 0.9, β is the FWHM in radians, and θ is half of the Bragg angle (2θ/2). Waste-derived Ag exhibited estimated crystallite sizes of 8.57–14.10 nm (12.08 nm in average), while Ag from $AgNO_3$ ranged from 6.36 to 13.04 nm (10.68 nm in average). XRD results (12.08 and 10.68 nm) indicate crystallite sizes, whereas TEM shows larger particles (38.40 and 24.48 nm), suggesting that AgNP is an aggregate of multiple crystallites [39].

The observed size discrepancies between XRD and TEM are consistent with previous reports on green-synthesized Ag using $AgNO_3$, which typically yield a crystallite size of ~10 nm by XRD and a particle size of ~20 nm by TEM [18]. Meanwhile, the quasi-spherical and polygonal nanoplatelet shapes suggest anisotropic growth, likely arising from three synergistic effects. Complexation of AgCl with NH_3 forming $[Ag(NH_3)_2]^+$ slows Ag^+ reduction due to lower free ion activity [40][41], thereby enabling ligand-directed growth; Chloride ions (Cl^-) released from AgCl can act as facet-selective agents, stabilizing certain crystallographic planes and thereby influencing anisotropic growth [42][43]. Such effects are considered to promote the development of (111)-dominated structures and may contribute to anisotropic shapes such as octahedra or nanoplatelets [44]. By contrast, in the $AgNO_3$ system, the absence of Cl^- under weakly adsorbing NO_3^- anions leads to more isotropic growth and predominantly quasi-spherical particles [45]. Phytochemicals in the extract, including polyphenols, act as mild reductants and capping agents, selectively adsorbing onto facets and modulating growth rates [41].

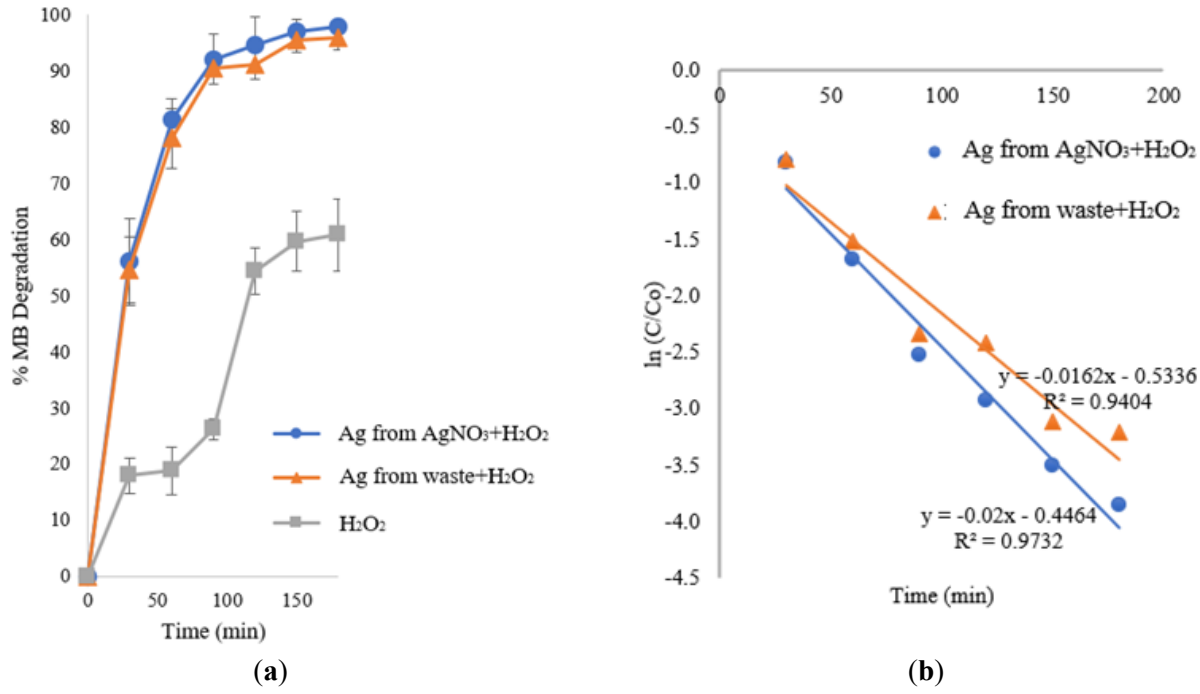

(**a**) (**b**)

Figure 5. (a) Degradation of methylene blue (MB) over time under different catalytic conditions: H_2O_2 + Ag from $AgNO_3$ (blue circles), H_2O_2 + Ag from waste (orange triangles), and H_2O_2 alone (gray squares). **(b)** First-order kinetic plots for the degradation of methylene blue (MB) using H_2O_2 with silver catalysts derived from $AgNO_3$ (blue circles) and waste Ag (orange triangles).

Table 4. Statistical analysis of methylene blue degradation efficiency across different.

Statistic test	System	Statistic	p-value
Saphiro Wilk test for normality	H_2O_2+Ag from $AgNO_3$	0.736	0.009
	H_2O_2+Ag from waste	0.746	0.011
	H_2O_2	0.882	0.235
Kruskal-Wallis test for the systems comparison	The three systems	5.9 (Chi squared)	0.052
Mann-Whitney U test	H_2O_2+Ag from $AgNO_3$ vs H_2O_2+Ag from waste	-	0.535 (n.s.)
	H_2O_2+Ag from $AgNO_3$ vs H_2O_2+Ag from waste	-	0.038
	H_2O_2+Ag from waste vs H_2O_2	-	0.038

n.s. = not significant

Beyond these mechanistic aspects, the size and shape of AgNPs can be deliberately tuned by adjusting synthesis parameters such as the precursor -to-extract ratio, pH, temperature, reaction time, and the presence of halide ions. A higher concentration of reducing phytochemicals or a lower metal salt concentration typically yields smaller nanoparticles [46], while pH and temperature strongly influence the nucleation–growth balance, leading to spherical, rod-like, or anisotropic shapes [47]. Halide ions, such as Cl^- , further modulate facet-selective growth and promote anisotropic morphologies [48]. Such control is essential, as smaller nanoparticles with a high surface-to-volume ratio enhance both catalytic and antimicrobial activity, whereas anisotropic shapes provide unique optical properties that are beneficial for sensing and photocatalysis.

Figure 4(b) presents the electrokinetic properties of AgNPs synthesized from waste and $AgNO_3$ under identical conditions. Waste-derived AgNPs exhibit a zeta potential of -30 mV and an electrophoretic mobility of -0.00023 cm^2/Vs, while $AgNO_3$-derived AgNPs show a zeta potential of -39 mV and an electrophoretic mobility of -0.00030 cm^2/Vs. The lower stability of waste-derived Ag^0 likely results from NH_3 acting as a weakly bound ligand, competing with plant-derived capping agents and reducing surface coverage, thereby weakening electrostatic repulsion. In contrast, Ag^+ from $AgNO_3$ (use no NH_3) binds directly with biomolecules, enhancing surface passivation and negative charge density. Both systems maintain colloidal stability despite differences, with a zeta potential > 30 mV [49]-[51].

3.3. Photocatalytic Test

Figure 5(a) illustrates the photocatalytic degradation of methylene blue under UV light, revealing significant efficiency differences among the three catalytic systems; the H_2O_2+Ag from waste shows comparable efficiency (96% degradation) in 180 min, H_2O_2+Ag system from $AgNO_3$ exhibits slightly higher photocatalytic activity in reducing methylene blue concentration to 97.9% degradation in 180 min that can be correlated with its smaller particle size, as observed in the material characterization, which enhances charge transfer and active site availability.

Even so, both AgNP systems exhibited higher photocatalytic activity than the H_2O_2-alone system (60.8%), indicating that the combination of AgNPs and H_2O_2 significantly enhances degradation. The 60.8% degradation of methylene blue by UV/H_2O_2 alone is due to the formation of hydroxyl radicals (•OH) via photolysis of H_2O_2 [52]. With the addition of AgNPs, the degradation is further enhanced, as AgNPs promote electron transfer that accelerates H_2O_2 decomposition into • OH. Upon UV irradiation, the localized surface plasmon resonance (LSPR) of AgNPs facilitates hot electron injection into the conduction band, enhancing H_2O_2 activation via electron transfer, generating hydroxyl radicals (•OH) and superoxide radicals ($O_2•^-$), which are highly reactive in breaking down

Table 5. Comparison with previous studies.

No	Ag precursor	Reductant	AgNP size (nm)	Morphology	Initial dye conc.	pH	%Removal	Catalyst dose	Reac. rate cons. (min^{-1})	Ref.
1.	Argento-metric waste	*Sandoricum koetjape* pericarp extract	38.4±1.39	Mostly polygonal nanoplatelets	50 ppm	7	96% MB	25 µg/mL	0.0162	This study
2.	$AgNO_3$	*Gardenia resinifera* leaf extract	70-100	Spherical	n.r.	n.r.	>88% MB	n.r.	n.r.	[57]
3.	$AgNO_3$	*Citrus aurantium* peel extract	9500	Cubic	n.r.	n.r.	95.35% MB and other dye	n.r.	n.r.	[58]
4	$AgNO_3$	*Cocos nucifera* husk fibre lignin extract	20-40	Spherical	$2x10^{-5}$ M	8	91.18% MB	15.2 µg/mL*	0.0678	[59]
5.	$AgNO_3$	Waste tea extract	45	Torispherical	2.5 ppm	7	>80%MB	30 µg/mL	n.r	[60]

n.r. : not reported

*By assuming complete reduction of Ag^+ to Ag^0, the AgNPs colloid synthesized from 50 mL of 1000 ppm silver nitrate and 50 mL of 1000 ppm sodium lignosulfonate (SLS) (from Cocos Nucifera husk fiber) solution had an estimated concentration of 0.3175 mg Ag^0/mL; therefore, the addition of 2 mL of this colloid into the photocatalytic reaction system (42 mL in total volume) corresponds to a final catalyst dose of approximately 15.12 µg/mL.

methylene blue molecules [53][54]. Additionally, AgNPs act as electron reservoirs, reducing recombination rates and prolonging ROS lifetimes, thereby sustaining higher photocatalytic efficiency [52][55]. Therefore, the presence of AgNPs significantly enhances the degradation efficiency of methylene blue. In contrast, the H_2O_2-alone system shows lower degradation due to its limited ability to generate •OH radicals without catalytic activation.

The kinetic analysis of methylene blue photodegradation (Figure 5(b)) confirms that both AgNP systems follow pseudo-first-order kinetics, suggesting that the reaction rate is directly proportional to the concentration of methylene blue, following the Langmuir-Hinshelwood mechanism, which is commonly observed in heterogeneous photocatalysis [56]. The apparent rate constants (k) for AgNPs from $AgNO_3$ and waste were determined to be 0.02 and 0.0162 min^{-1}, respectively, indicating comparable reaction rates.

Statistical analysis (Table 4) reveals that the Shapiro-Wilk test indicates a non-normal distribution for H_2O_2+Ag from $AgNO_3$ ($p = 0.009$) and waste-derived AgNPs ($p = 0.011$) thus, the Kruskal-Wallis test was used to analyze the three systems. The overall comparison among these systems approaches statistical significance (chi-squared value of 5.9, $p = 0.052$), indicating a strong trend toward differing degradation efficiencies. Follow-up Mann–Whitney U tests confirm the source of this trend, showing that AgNP systems outperform H_2O_2 alone ($p = 0.038$ for each comparison). In contrast, the difference between AgNPs derived from $AgNO_3$ and waste is not significant ($p = 0.535$). Hence, the addition of AgNPs (regardless of their source) significantly enhances the degradation of methylene blue. Although $AgNO_3$-derived AgNPs exhibit a slightly higher mean efficiency (97.9 % vs 96 %), the difference is statistically insignificant ($p > 0.05$), indicating that both nanoparticles exhibit sufficient SPR effects and ROS generation capability, resulting in statistically equivalent photocatalytic activity.

Table 5 compares AgNPs synthesised from $AgNO_3$ and argentometric waste using a range of plant extracts. The argentometric waste route employing *S. koetjape* pericarp produced polygonal nanoplatelets capable of removing 96% of methylene blue. Meanwhile, AgNPs synthesised from $AgNO_3$ with *Gardenia resinifera* leaves or with waste-tea extract yielded spherical or torispherical particles, and *Citrus aurantium* peel extract produced cubic particles. Although their morphologies differ, the waste-derived AgNPs display photocatalytic activity comparable to that of other green-synthesized counterparts that used $AgNO_3$.

4. CONCLUSIONS

This study investigates the green synthesis of silver nanoparticles (Ag^0) using *Sandoricum koetjape* fruit pericarp extract and recycled silver waste from argentometric analysis, which is converted into diaminargentate. The extract provides hydroxyl (OH) and carbonyl (C=O) groups as reducing agents, while C=C, C–O/C–N, and OH groups potentially serve as capping agents. Waste-derived Ag^0 predominantly forms polygonal nanoplatelet crystals (~38.41 nm), whereas under the same reaction conditions, $AgNO_3$-derived Ag^0 yields mainly spherical nanoparticles (~24.48 nm). Both samples exhibit a face-centered cubic (FCC) structure, with the waste-derived Ag^0 displaying higher crystallinity. The nanoparticles exhibit good colloidal stability and achieve a methylene blue photodegradation efficiency of over 96%. These results highlight the valorization of argentometric laboratory waste into silver nanoparticles, exemplifying circular economy principles by closing the resource loop. This strategy not only reduces the environmental risks associated with silver disposal but also replaces conventional precursors, such as $AgNO_3$, with a sustainable, low-cost alternative that offers comparable performance in environmental remediation. This approach promotes waste minimization, resource efficiency, and the production of green nanomaterials.

AUTHOR INFORMATION

Corresponding Author

Endang Tri Wahyuni — Department of Chemistry, Universitas Gadjah Mada, Yogyakarta-55281 (Indonesia);

orcid.org/0000-0002-0584-0549

Email: endang_triw@ugm.ac.id

Authors

Mai Anugrahwati — Department of Chemistry, Universitas Gadjah Mada, Yogyakarta-55281 (Indonesia); Department of Chemistry, Universitas Islam Indonesia, Yogyakarta-55584 (Indonesia);

orcid.org/0000-0001-8031-8702

Sri Sudiono — Department of Chemistry, Universitas Gadjah Mada, Yogyakarta-55281 (Indonesia);

orcid.org/0000-0001-5024-7114

Author Contributions

Conceptualization, Methodology, Validation, Writing – Review & Editing, E. T. W., S. S., and M. A.; Formal Analysis, Investigation, Resources, Software, Funding Acquisition, and Data Curation, M. A.; Writing – Original Draft Preparation, M. A. and E. T. W.; Supervision, E. T. W. and S. S.

Conflicts of Interest

The authors declare no conflict of interest.

ACKNOWLEDGEMENT

The authors gratefully acknowledge financial support from the Indonesian Endowment Fund for Education (Lembaga Pengelola Dana Pendidikan, LPDP) through a scholarship for Mai Anugrahwati to pursue doctoral studies at Universitas Gadjah Mada (2022–2026) and funding for this research.

DECLARATION OF GENERATIVE AI

Not applicable.

REFERENCES

[1] M. Abass Sofi, S. Sunitha, M. Ashaq Sofi, S. K. Khadheer Pasha, and D. Choi. (2022). "An overview of antimicrobial and anticancer potential of silver nanoparticles". *Journal of King Saud University - Science.* **34** (2). 10.1016/j.jksus.2021.101791.

[2] T. S. Institute. (2024). "Global silver demand forecasted to rise to 1.2 bn ounces in 2024". *Focus on Catalysts.* **2024** (3). 10.1016/j.focat.2024.02.014.

[3] E. Mining. (2024). "Industrial demand for silver reaches record levels". *Focus on Catalysts.* **2024** (8).10.1016/j.focat.2024.07.008.

[4] G. Chavez-Esquivel, H. Cervantes-Cuevas, D. E. Cortes-Cordova, P. Estrada de los Santos, and L. Huerta Arcos. (2024). "Silver-doped graphite oxide composites used as antimicrobial agents against Staphylococcus aureus, Escherichia coli and Tatumella terrea evaluated by direct TLC bioautography". *Nano Express.* **5** (1). 10.1088/2632-959X/ad2998.

[5] J. Sarkar, A. Naskar, A. Nath, B. Gangopadhyay, E. Tarafdar, D. Das, S. Chakraborty, D. Chattopadhyay, and K. Acharya. (2024). "Innovative utilization of harvested mushroom substrate for green synthesis of silver nanoparticles: A multi-response optimization approach". *Environmental Research.* **248** : 118297. 10.1016/j.envres.2024.118297.

[6] M. Pradeep, D. Kruszka, P. Kachlicki, D. Mondal, and G. Franklin. (2021). "Uncovering the Phytochemical Basis and the Mechanism of Plant Extract-Mediated Eco-Friendly Synthesis of Silver Nanoparticles Using Ultra-Performance Liquid Chromatography Coupled with a Photodiode Array and High-Resolution Mass Spectrometry". *ACS Sustainable Chemistry & Engineering.* **10** (1): 562-571. 10.1021/acssuschemeng.1c06960.

[7] Y. K. Mohanta, A. K. Mishra, J. Panda, I. Chakrabartty, B. Sarma, S. K. Panda, H. Chopra, G. Zengin, M. G. Moloney, and M. Sharifi-Rad. (2023). "Promising applications of phyto-fabricated silver nanoparticles: Recent trends in biomedicine". *Biochemical and Biophysical Research Communications.* **688** : 149126. 10.1016/j.bbrc.2023.149126.

[8] G. Gusrizal, T. A. Zaharah, A. Shofiyani, and S. J. Santosa. (2021). "Waste from Argentometric Determination of Chloride as a Source of Silver in the Synthesis of p-Hydroxybenzoic Acid Capped Silver Nanoparticles". *ChemistrySelect.* **6** (23): 5763-5770. 10.1002/slct.202004184.

[9] M. S. Mondal, A. Paul, and M. Rhaman. (2023). "Recycling of silver nanoparticles from electronic waste via green synthesis and application of AgNPs-chitosan based nanocomposite on textile material". *Scientific Reports.* **13** (1): 13798. 10.1038/s41598-023-40668-7.

[10] A. Singhal and A. Gupta. (2019). "Sustainable synthesis of silver nanoparticles using exposed X-ray sheets and forest-industrial waste biomass: Assessment of kinetic and catalytic properties for degradation of toxic dyes mixture". *Journal of Environmental Management.* **247** : 698-711. 10.1016/j.jenvman.2019.06.078.

[11] M. S. Bures, L. Maslov Bandic, and K. Vlahovicek-Kahlina. (2023). "Determination of Bioactive Components in Mandarin Fruits: A Review". *Critical Reviews in Analytical Chemistry.* **53** (7): 1489-1514. 10.1080/10408347.2022.2035209.

[12] M. A. Rasadah, S. Khozirah, A. A. Aznie, and M. M. Nik. (2004). "Anti-inflammatory agents from Sandoricum koetjape Merr". *Phytomedicine.* **11** (2-3): 261-3. 10.1078/0944-7113-00339.

[13] S. Saadah, S. M. Tulandi, and R. A. Rohman. (2023). "Seven types of phenolic acid and inhibitory activity for protein tyrosine phosphatase 1B (PTP1B) from the stem of Sandoricum koetjape". *IOP Conference Series: Earth and Environmental Science.* **1255** (1). 10.1088/1755-1315/1255/1/012070.

[14] I. N. Wirata, A. A. G. Agung, N. W. Arini, I. G. A. Raiyanti, I. K. Aryana, and I. N. Purna. (2023). "Decrease in the number of Streptococcus mutans and Staphylococcus aureus bacterial colonies after administration of sentul fruit peel extract gel (Sandoricum koetjape) in gingivitis model of white Wistar rats". *Bali Medical Journal.* **12** (3): 2739-2742. 10.15562/bmj.v12i3.4753.

[15] A. S. Rini, Y. Rati, and S. W. Maisita. (2021). "Of ZnO Nanoparticle using Sandoricum Koetjape Peel Extract as Bio-stabilizer under Microwave Irradiation". *Journal of Physics: Conference Series.* **2049** (1). 10.1088/1742-6596/2049/1/012069.

[16] A. Najafi, M. Khoeini, G. Khalaj, and A. Sahebgharan. (2021). "Synthesis of silver nanoparticles from electronic scrap by chemical reduction". *Materials Research Express.* **8** (12). 10.1088/2053-1591/ac406d.

[17] Y. Medina Castillo, L. F. Cárdenas Guevara, R. J. Rincón, G. A. Murillo Romero, J. Niño Abella, J. Amaya, and D. Llamosa Perez. (2024). "Comparative evaluation of antibacterial efficacy of silver nanoparticles synthesized with Cannabis sativa extract at different concentrations". *Applied Nanoscience.* **14** (12): 1139-1155. 10.1007/s13204-024-03073-8.

[18] A. S. Rini, A. Fitrisia, Y. Rati, L. Umar, and Y. Soerbakti. (2023). "Bio-Colloidal Silver Nanoparticles Prepared via Green Synthesis Using Sandoricum koetjape Peel Extract for Selective Colorimetry-Based Mercury Ions Detection". *Karbala International Journal of Modern Science.* **9** (2). 10.33640/2405-609x.3299.

[19] A. Fatiqin, R. Alfanaar, S. Rahman, Y. Febrianto, S. Citrariana, M. a. P. Arsana, T. Suprayogi, and Y. S. Kurniawan. (2024). "Catalytic Reduction of 4-Nitrophenol and Methylene Blue with Silver Nanoparticles Decorated with Drymoglossum piloselloides Extract". *Journal of Multidisciplinary Applied Natural Science.* **4** (2): 249-261. 10.47352/jmans.2774-3047.210.

[20] H. Zaid, Z. Al-sharify, M. H. Hamzah, and S. Rushdi. (2022). "Optimization of Different Chemical Processes Using Response Surface Methodology- a Review". *Journal of Engineering and Sustainable Development.* **26** (6): 1-12. 10.31272/jeasd.26.6.1.

[21] G. Nikaeen, S. Yousefinejad, S. Rahmdel, F. Samari, and S. Mahdavinia. (2020). "Central Composite Design for Optimizing the Biosynthesis of Silver Nanoparticles using Plantago major Extract and Investigating Antibacterial, Antifungal and Antioxidant Activity". *Scientific Reports.* **10** (1): 9642. 10.1038/s41598-020-66357-3.

[22] K. R. A. Javier and D. H. Camacho. (2022). "Dataset on the optimization by response surface methodology for the synthesis of silver nanoparticles using Laxitextum bicolor

mushroom". *Data Brief.* **45** : 108631. 10.1016/j.dib.2022.108631.

[23] V. L. Sanches, L. M. de Souza Mesquita, J. Vigano, L. S. Contieri, R. Pizani, J. Chaves, L. C. da Silva, M. C. de Souza, M. C. Breitkreitz, and M. A. Rostagno. (2024). "Insights on the Extraction and Analysis of Phenolic Compounds from Citrus Fruits: Green Perspectives and Current Status". *Critical Reviews in Analytical Chemistry.* **54** (5): 1173-1199. 10.1080/10408347.2022.2107871.

[24] R. D. Hardini and T. E. Saraswati. (2023). "Concentration dependence of NaBH4reductant on the optical properties of colloidal silver nanoparticles synthesized from AgNO3solution". *Journal of Physics: Conference Series.* **2556** (1). 10.1088/1742-6596/2556/1/012013.

[25] S. Menon, A. R. Jose, S. Jesny, and K. G. Kumar. (2016). "A colorimetric and fluorometric sensor for the determination of norepinephrine". *Analytical Methods.* **8** (29): 5801-5805. 10.1039/c6ay01539e.

[26] N. Tarannum, Divya, and Y. K. Gautam. (2019). "Facile green synthesis and applications of silver nanoparticles: a state-of -the-art review". *RSC Advances.* **9** (60): 34926-34948. 10.1039/c9ra04164h.

[27] A. H. E. Moustafa, M. A. Mousa, H. H. Abdelrahman, M. A. Fahmy, and D. G. Ebrahim. (2023). "A novel successful strategy for the detection of antibiotics and toxic heavy metals based on fluorescence silver/graphene quantum dots nanocomposites". *Applied Nanoscience.* **14** (1): 1-20. 10.1007/s13204-023-02921-3.

[28] T. Arfin, Sonawane, and K. Arshiya Tarannum. (2019). "Review on Detection of Phenol in Water ". *Advanced Materials Letters.* **10** (11): 753-785. 10.5185/amlett.2019.0036.

[29] C. Astutiningsih, T. E. Rahmawati, N. A. Rahman, and M. Meri. (2024). "Green Synthesis of ZnO Nanoparticles using Abelmoschus esculenthus L. Fruit Extract: Antioxidant, Photoprotective, Anti-inflammatory, and Antibacterial Studies". *Journal of Multidisciplinary Applied Natural Science.* **4** (1): 176-193. 10.47352/jmans.2774-3047.204.

[30] Wendelim and B. L. Fibriarti. (2024). "The Potential of Sentul (Sandoricum koetjape) Fruit Skin Endophytic Bacteria as an Antifungal for Ganoderma boninense". *Jurnal Biologi Indonesia.* **20** (2): 111-120. 10.47349/jbi/20022024/111.

[31] S. G. B. de Souza, K. J. S. Silva, M. M. R. Azevedo, A. K. O. Lima, H. de Campos Braga, D. B. Tada, K. Gul, S. Malik, G. Nakazato, and P. S. Taube. (2023). "Green synthesis and characterization of honey-mediated silver nanoparticles". *Applied Nanoscience.* **14** (1): 191-201. 10.1007/s13204-023-02969-1.

[32] A. Kumari Das, S. Neupane, K. Kumar Nayak, S. Shrestha, N. Karki, D. Kumar Gupta, and A. Prasad Yadav. (2024). "Dichloromethane -Methanol fraction of Mahonia nepalensis containing Berberine, Jatrorrhizine, and Tetrahydroberberine as corrosion inhibitor for mild steel". *Results in Chemistry.* **12**. 10.1016/j.rechem.2024.101866.

[33] S. K. Moutari, A. M. Abdoulkadri, A. S. Boulhassane, A. Rabani, and I. Khalid. (2018). "Determination Contents of Total Phenolic Pigments and Spectrophotometric Characterization of Crude Extracts of Ten Tinctorial Plants of Niger which is Usable in Solar Energy". *European Scientific Journal, ESJ.* **14** (33). 10.19044/esj.2018.v14n33p389.

[34] M. Szymczak, J. A. Pankowski, A. Kwiatek, B. Grygorcewicz, J. Karczewska-Golec, K. Sadowska, and P. Golec. (2024). "An effective antibiofilm strategy based on bacteriophages armed with silver nanoparticles". *Scientific Reports.* **14** (1): 9088. 10.1038/s41598-024-59866-y.

[35] N. M. Jassim. (2024). "Synthesis and nonlinear optical responses of Ag: ZnO core: shell nanoparticles induced by Z-scan technique". *Journal of Optics.* 10.1007/s12596-024-02432-6.

[36] R. González-Campuzano, J. Delgado-Aguillón, R. Y. Sato-Berrú, A. Sainz-Vidal, A. A. Rodríguez-Rosales, C. J. Román-Moreno, and J. Garduño-Mejía. (2023).

"Saturable absorption and negative nonlinear refraction index evolution in silver nanoparticles colloids". *Optics & Laser Technology.* **159**. 10.1016/j.optlastec.2022.108989.

[37] A. Amirjani, F. Firouzi, and D. F. Haghshenas. (2020). "Predicting the Size of Silver Nanoparticles from Their Optical Properties". *Plasmonics.* **15** (4): 1077-1082. 10.1007/s11468-020-01121-x.

[38] B. Syed, N. N. M, L. D. B, M. K. K, Y. S, and S. S. (2016). "Synthesis of silver nanoparticles by endosymbiont Pseudomonas fluorescens CA 417 and their bactericidal activity". *Enzyme and Microbial Technology.* **95** : 128-136. 10.1016/j.enzmictec.2016.10.004.

[39] J. Helmlinger, O. Prymak, K. Loza, M. Gocyla, M. Heggen, and M. Epple. (2016). "On the Crystallography of Silver Nanoparticles with Different Shapes". *Crystal Growth & Design.* **16** (7): 3677-3687. 10.1021/acs.cgd.6b00178.

[40] Y. Xia, Y. Xiong, B. Lim, and S. E. Skrabalak. (2009). "Shape-controlled synthesis of metal nanocrystals: simple chemistry meets complex physics?". *Angewandte Chemie International Edition in English.* **48** (1): 60-103. 10.1002/anie.200802248.

[41] J. Zeng, Y. Zheng, M. Rycenga, J. Tao, Z. Y. Li, Q. Zhang, Y. Zhu, and Y. Xia. (2010). "Controlling the shapes of silver nanocrystals with different capping agents". *Journal of the American Chemical Society.* **132** (25): 8552-3. 10.1021/ja103655f.

[42] Z. Chen, T. Balankura, K. A. Fichthorn, and R. M. Rioux. (2019). "Revisiting the Polyol Synthesis of Silver Nanostructures: Role of Chloride in Nanocube Formation". *ACS Nano.* **13** (2): 1849-1860. 10.1021/acsnano.8b08019.

[43] Z. Chen, J. W. Chang, C. Balasanthiran, S. T. Milner, and R. M. Rioux. (2019). "Anisotropic Growth of Silver Nanoparticles Is Kinetically Controlled by Polyvinylpyrrolidone Binding". *Journal of the American Chemical Society.* **141** (10): 4328-4337. 10.1021/jacs.8b11295.

[44] F. Kim, S. Connor, H. Song, T. Kuykendall, and P. Yang. (2004). "Platonic gold nanocrystals". *Angewandte Chemie International Edition in English.* **43** (28): 3673-7. 10.1002/anie.200454216.

[45] S. Ghosh and L. Manna. (2018). "The Many "Facets" of Halide Ions in the Chemistry of Colloidal Inorganic Nanocrystals". *Chemical Reviews.* **118** (16): 7804-7864. 10.1021/acs.chemrev.8b00158.

[46] A. Fatiqin, H. Amrulloh, W. Simanjuntak, I. Apriani, R. A. H. T. Amelia, Syarifah, R. N. Sunarti, and A. R. P. Raharjeng. (2021). "Characteristics of nano-size MgO prepared using aqueous extract of different parts of Moringa oleifera plant as green synthesis agents". *AIP Conference Proceedings.* 10.1063/5.0041999.

[47] Y. C. Lee, S. J. Chen, and C. L. Huang. (2013). "Finding a Facile Method to Synthesize Decahedral Silver Nanoparticles through a Systematic Study of Temperature Effect on Photomediated Silver Nanostructure Growth". *Journal of the Chinese Chemical Society.* **57** (3A): 325-331. 10.1002/jccs.201000048.

[48] J. Tang, Q. Zhao, N. Zhang, and S. Q. Man. (2015). "Citrate ions and chloride ions involved in the synthesis of anisotropic silver nanostructures". *Micro & Nano Letters.* **10** (2): 71-75. 10.1049/mnl.2014.0185.

[49] L. R. Pokhrel, B. Dubey, and P. R. Scheuerman. (2013). "Impacts of select organic ligands on the colloidal stability, dissolution dynamics, and toxicity of silver nanoparticles". *Environmental Science & Technology.* **47** (22): 12877-85. 10.1021/es403462j.

[50] E. A. Kyriakidou, O. S. Alexeev, A. P. Wong, C. Papadimitriou, M. D. Amiridis, and J. R. Regalbuto. (2016). "Synthesis of Ag nanoparticles on oxide and carbon supports from Ag diammine precursor". *Journal of Catalysis.* **344** : 749-756. 10.1016/j.jcat.2016.08.018.

[51] Z. Nemeth, I. Csoka, R. Semnani Jazani, B. Sipos, H. Haspel, G. Kozma, Z. Konya, and D. G. Dobo. (2022). "Quality by Design-Driven Zeta Potential Optimisation Study of

Liposomes with Charge Imparting Membrane Additives". *Pharmaceutics.* **14** (9). 10.3390/pharmaceutics14091798.

[52] J. Jiao, J. Wan, Y. Ma, and Y. Wang. (2019). "Enhanced photocatalytic activity of AgNPs-in-CNTs with hydrogen peroxide under visible light irradiation". *Environmental Science and Pollution Research.* **26** (25): 26389-26396. 10.1007/s11356-019-05877-6.

[53] D. He, A. M. Jones, S. Garg, A. N. Pham, and T. D. Waite. (2011). "Silver Nanoparticle−Reactive Oxygen Species Interactions: Application of a Charging−Discharging Model". *The Journal of Physical Chemistry C.* **115** (13): 5461-5468. 10.1021/jp111275a.

[54] J. Thomas, P. Periakaruppan, V. Thomas, J. John, M. S, T. Thomas, J. Jose, R. I, and M. A. (2018). "Morphology dependent nonlinear optical and photocatalytic activity of anisotropic plasmonic silver". *RSC Advances.* **8** (72): 41288-41298. 10.1039/c8ra08893d.

[55] F. Meng, X. Zhu, and P. Miao. (2015). "Study of autocatalytic oxidation reaction of silver nanoparticles and the application for nonenzymatic H2O2 assay". *Chemical Physics Letters.* **635** : 213-216. 10.1016/j.cplett.2015.06.068.

[56] M. M. Martin, J. R. E. Sumayao, A. N. Soriano, and R. V. C. Rubi. (2023). "Photocatalytic Degradation Activity of the Biosynthesized R. rosifolius Mediated Silver Nanoparticles in Methylene Blue Dye". *ASEAN Journal of Chemical Engineering.* **23** (3). 10.22146/ajche.82506.

[57] S. K. Urumbil, E. J. Jesy, A. J. Jasmine Mariya, and K. B. Sherin. (2024). "Biosynthesis and Characterisation of Silver Nanoparticles using Leaf Extract of Gardenia resinifera and its Antioxidant and Photocatalytic Degradation Activity". *Journal of Natural Remedies.* 2451-2458. 10.18311/jnr/2024/41904.

[58] S. Ringwal, A. S. Bartwal, and S. C. Sati. (2021). "Photo-catalytic degradation of different toxic dyes using silver nanoparticles as photo-catalyst, mediated via Citrus aurantium peels extract". *Journal of the Indian Chemical Society.* **98** (12). 10.1016/j.jics.2021.100221.

[59] N. Arifah Binti Ahmad Che Hamat, A. Phaik-Ching, M. Nasir Mohamad Ibrahim, N. H. H. Abu Bakar, T.-W. Tan, N. Farhanah Binti Mohd Amin, Z. N. Garba, V. Perumal, and P. Bothi Raja. (2024). "Cocos Nucifera's lignin mediated silver nanoparticle and their photocatalytic activity". *Inorganic Chemistry Communications.* **160**. 10.1016/j.inoche.2023.111845.

[60] W. Qing, K. Chen, Y. Wang, X. Liu, and M. Lu. (2017). "Green synthesis of silver nanoparticles by waste tea extract and degradation of organic dye in the absence and presence of H2O2". *Applied Surface Science.* **423** : 1019-1024. 10.1016/j.apsusc.2017.07.007.